Validation of the ICE-3G Model of Würm-Wisconsin Deglaciation Using a Global Data Base of Relative Sea Level Histories

A. M. TUSHINGHAM[1] AND W. R. PELTIER

Department of Physics, University of Toronto, Toronto, Ontario, Canada

A global data base consisting of radiocarbon-controlled relative sea level (RSL) histories from 392 different geographic locations has been compiled for use in analyses of the glacial isostatic adjustment process. These data may be employed to constrain both the spatiotemporal characteristics of the last deglaciation event of the current ice age and the rheological structure of the planetary interior. In a previous paper in this series (Tushingham and Peltier, 1991), we employed the RSL data in this set from sites that were once ice covered to refine the apriori model of deglaciation that had been delivered by past research in the area of Pleistocene geomorphology (Peltier and Andrews, 1976; Wu and Peltier, 1983) to produce a new global model of this event that we have called ICE-3G. In the present paper, following a description of the full data base and of the methods used to compile it, we employ data from the sites that were not ice covered (200 time series) to verify the plausibility of this refined model of deglaciation and to test the extent to which the totality of the observations constrain the radial viscoelastic structure of the planet. The analysis of solutions to the forward problem presented here reinforce previous inferences of a preference for a thick lithosphere by RSL data from sites along the U.S. east coast and a preference by data from most near-field sites for an increase in viscosity across the 670-km discontinuity in the mantle by a factor of approximately 2, when the viscosity of the upper mantle is fixed to the value of 10^{21} Pa s originally deduced by Haskel (1935) on the basis of his analysis of the data from Fennoscandia.

1. INTRODUCTION

The inference of mantle viscosity, from observations of the Earth's response to the 10^5 year glaciation-deglaciation cycle that has characterized the last 900,000 years of the current ice age [e.g., *Shackleton et al.*, 1990], remains a problem of considerable geophysical interest. Although a number of alternative observational constraints exist that can be employed to bound this important Earth property, these are inevitably inferior to those connected with the glacial isostatic adjustment process. Nonhydrostatic geoid anomalies, for example, have been invoked by *Hager* [1984] and *Richards and Hager* [1984] in conjunction with models of the lateral heterogeneity of the mantle density field provided by seismic tomography to argue that the lower mantle has a much higher viscosity than the upper mantle. As pointed out by *Forte and Peltier* [1987, 1989, 1991a,b], however, this argument is undermined by virtue of the fact that the data have been inverted only in terms of poloidal models of the mantle convection process, whereas surface plate kinematics reveals a near equipartition of kinetic energy between poloidal and toroidal components. Because the postglacial rebound phenomenon is considerably less complex geometrically than is mantle convection and because the variation in the distribution of surface mass associated with deglaciation that drives the process is very much better constrained than the internal lateral heterogeneity of density that drives mantle convection, it should be clear that glacial isostatic adjustment data will provide much less ambiguous information on mantle viscosity than that related to the convection process.

A principle difficulty that must be faced in attempting to extract unambiguous inferences concerning mantle viscosity from postglacial rebound data is nevertheless associated with imprecision in our knowledge of the deglaciation process. That is,

we do not know with certainty the variations of continental ice thickness with time since glacial maximum. In fact, there is continuing debate as to whether significant continental ice sheets even existed in certain regions (e.g., Siberia, Tibet, Alaska, the Queen Elizabeth Islands of Arctic Canada; see *Tushingham and Peltier* [1991] for a recent review). Until very recently, estimates of the history of continental deglaciation had been produced solely on the basis of ice mechanical considerations that employed the assumption of steady state conditions [e.g., *Denton and Hughes*, 1981] or were ad hoc models fit to the known locations of the retreat moraines of individual ice masses with ice thicknesses determined very crudely (e.g., the ICE-1 model of *Peltier and Andrews* [1976]). Very recently, these approximate models have been considerably refined by *Tushingham and Peltier* [1991], who have used a very extensive compilation of radiocarbon-controlled relative sea level (RSL) histories from ice covered regions and a theoretical model of the glacial isostatic adjustment process to improve the deglaciation model by adjusting it to optimize the fit of the theory to the observations. Since this requires that the radial viscoelastic structure of the Earth be assumed known, and since this is most strongly constrained by the data from ice covered regions, there is clearly an element of circularity to the argument and we must be concerned as to whether other, perhaps equally plausible, combinations of deglaciation history and radial viscoelastic structure might prove equally capable of reconciling the observations.

Our purpose in the present paper is to investigate from at least one further perspective the issue of the global self-consistency of the combination of mantle viscoelastic structure and deglaciation history that was demonstrated by *Tushingham and Peltier* [1991] to fit the relative sea level data from ice covered regions extremely accurately. This will involve examination of the fits of the model to RSL data from regions that were not ice covered and therefore were not employed to refine the deglaciation history. As we will see, these analyses will confirm the global consistency of the previously determined models of deglaciation history and radial viscoelastic structure. An extremely interesting aspect of these

[1]Now at Geodynamics Section, Geological Survey of Canada, Ottawa, Ontario, Canada.

comparisons between theory and observations at sites remote from the centres of northern hemisphere glaciation concerns RSL data from a few sites for which the records extend back in time to glacial maximum. In this connection the recently published data from Barbados corals [*Fairbanks*, 1989] with age control based upon the uranium-thorium method [*Bard et al.*, 1990] will prove especially important.

The plan of this paper is therefore as follows. In section 2 we will briefly discuss the problems encountered in using relative sea level records based upon the application of radiocarbon dating methods in reference to a new sea level curve that we have obtained for Thores River, Ellesmere Island, Arctic Canada. Following this, the complete data base of RSL curves that we have assembled for use in this work is presented (see listing in Appendices A and B on microfiche[1]). Section 3 is devoted to a presentation of the fits of the theoretical model to the observations at non-ice-covered sites. The theoretical model that we employ has been reviewed in detail very recently [*Peltier*, 1989], and we will therefore provide no further comment on it here. Given the quality of these fits of theory to data, we continue in section 4 to perform a number of sensitivity tests in order to estimate through analyses of the forward problem the quality of the constraints on mantle viscosity structure that RSL data from various locations on the Earth's surface may be invoked to provide. Our conclusions are presented in section 5.

2. A RELATIVE SEA LEVEL DATA BASE FOR GLACIAL ISOSTATIC ADJUSTMENT ANALYSIS

In using relative sea level data for the purpose of constraining geophysical models there are a number of issues that must be kept clearly in mind. These concern both the meaning that is to be attached to various sea level indicators and the methods that are employed to determine their true sidereal age from the measured radiocarbon age. Since considerable recent progress has been made in connection with the latter question, we will pay special attention to it in the discussion that follows. Our main goal in this section is to provide a detailed discussion of the methods that we have employed in compiling and using the RSL data base that we shall present.

---

[1]Appendices A and B are available with entire article on microfiche. Order from American Geophysical Union, 2000 Florida Ave., N.W., Washington, D.C. 20009. Document B91-005; $2.50. Payment must accompany order.

2.1. *Observations of Variations in Relative Sea Level*

In order to constrain the global scale glacial isostatic adjustment that has been occurring since the onset of the last major deglaciation event, it is clearly necessary to compile a global collection of relative sea level data. Each RSL history is inferred from geological samples collected in the field, usually consisting of organic materials found in or near relict shorelines located at various elevations above or below present-day sea level. Wave action, marine deposition, and terrestrial deposition are the three different processes which form features that may indicate the presence of a relict shoreline, as outlined in many standard texts in geomorphology [e.g., *Bird*, 1967; *Flint*, 1971].

Regardless of the geological feature being examined, we clearly require a method of estimating its age in order to use the feature to constrain relative sea level. Early methods such as varve chronology and pollen analysis have been superceded by radiocarbon analysis [*Libby*, 1955]. To obtain a radiocarbon estimate of the age of the RSL indicator feature, any organic or carbonate material found in or near the feature (such as a marine shell, a piece of driftwood, a drowned tree stump, peat, a microfossil, or whale or polar bear bone) may be collected and analyzed. It is essential that the material can be stratigraphically associated with the RSL indicator feature in such a way that the timing of the deposition of the material can be assumed to correspond to the time of the formation of the feature. In the field this is often difficult to ascertain. Early work in constructing RSL histories using radiocarbon-dated relict shorelines was undertaken in the early 1960s by *Curray* [1960] in the Gulf of Mexico, *Redfield and Rubin* [1962] in New England, *Washburn and Stuiver* [1962] in Greenland, and *Olsson and Blake* [1962] in Spitsbergen. Since then, and especially over the last decade, the quantity and quality of radiocarbon-controlled RSL data has grown dramatically. The application of accelerator mass spectrometry (AMS) to ^{14}C dating has contributed greatly to this improvement.

Whereas earlier methods (e.g., varve chronologies) allowed age estimates to be obtained in sidereal years, radiocarbon methods do not. Due to fluctuations of cosmic ray intensity and of the strength of the Earth's magnetic field the radiocarbon timescale is not the same as the sidereal timescale so an atmospheric radiocarbon calibration curve, such as the conventional one presented in Figure 1a is required. This curve from the present back to 7 kyr B.P. is based on a tree ring study of Irish Oaks by *Pearson et al.* [1986], and is extended to 8 kyr B.P. using *Stuiver et al.*s [1986]
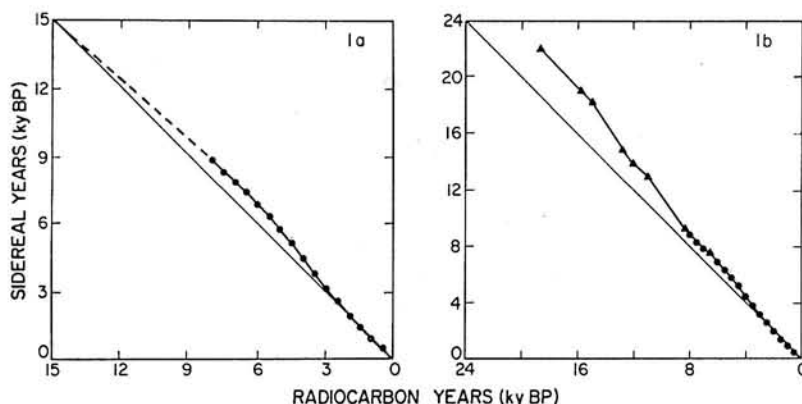

Fig. 1. (*a*) Atmospheric ^{14}C correction curves. This curve, which converts radiocarbon years into sidereal years, was based on tree ring studies from the present back to 7 kyr B.P. [*Pearson et al.*, 1986]. Using a model of marine ^{14}C trends [*Stuiver et al.*, 1986], the curve was extended to 8 kyr B.P. A further extension was obtained by employing the assumption that 15 kyr B.P. (radiocarbon) equals 15 kyr B.P. (sidereal). The dots show the data used in constructing the curve. (*b*) ^{14}C correction curve from the U-Th analysis of Barbadian corals by *Bard et al.* [1990].

model of marine ^{14}C trends and assuming marine trends parallel atmospheric trends, which appears valid for the last 8000 years. A major recent advance in the radiocarbon dating of late glacial and postglacial processes has been achieved using the new suite of Barbadian corals recovered by *Fairbanks* [1989] that provide a continuous sampling of RSL history at this site since the onset of deglaciation. *Bard et al.* [1990] have successfully employed uranium-thorium dating to accurately determine the age of these corals and compared them to ^{14}C dates obtained using AMS. This comparison recovers the tree ring constrained portion of the calibration curve but allows it to be extended back to 18,000 ^{14}C years to produce the new calibration curve shown in Figure 1b. As we will see in the analyses to follow, although most of the RSL data that we shall analyze are younger than 8000 ^{14}C years and therefore fall on the part of the calibration curve controlled by the tree ring chronology, there do exist data from some RSL sites that extend further back in time through the period for which the new U-Th dating control is required. At such sites the recalibrated data will be shown to fit the theoretical predictions of the global model whereas the uncalibrated data do not.

2.2. *Glacial Rebound at Thores River*

Before we discuss the methods employed to assemble the full global RSL data set, new and previously unpublished data from Thores River, northernmost Ellesmere Island, North West Territories, Canada, will be presented in order to describe how RSL data are typically collected in the field and thereby to
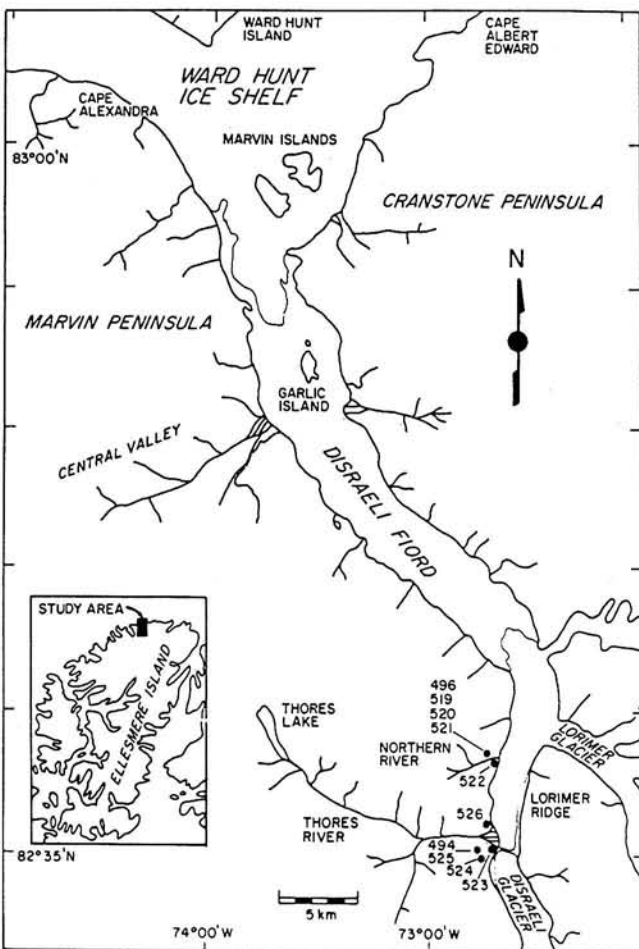
illustrate some of the problems that may occur. Experience obtained in the construction of this RSL curve provides a number of very valuable insights into the quality of the RSL data available in the literature.

The Thores River site on which we shall focus for the purpose of illustration is a large prograded marine delta located on the west side of the head of Disraeli Fiord (refer to Figure 2 for site location map) and is composed of five distinct deltas bisected by the modern Thores River. The flight of deltas on the south side of Thores River is labelled by the letters A-E and have elevations of 10, 15, 30, 51, and 68 m above sea level, respectively (as shown on Figure 3). (Only deltas A-C were preserved on the north side). The modern river has exposed a large section on the southern half of the delta in which the prograding sediment layers can easily be identified. There is, however, a horizontal feature beneath delta E which cuts through the prograded bedding and appears to be a continuation of the surface of delta D. If this feature is not stratigraphic in nature, delta E can be interpreted as being older than delta D and the entire flight of deltas could simply be indicators of a falling relative sea level. If, on the other hand the feature is stratigraphic, then delta E would have to be younger than delta D. This would indicate a 17-m rise in relative sea level. According to glacial isostatic calculations described by *Tushingham and Peltier* [1991], relative sea level in this area is expected to be monotonically falling (see Figure 3). The solid curve on Figure 3 is based on the thick Innuitian Ice Sheet of the ICE-3G reconstruction derived by *Tushingham and Peltier* [1991], while the dashed curve is based on the thin ice cover model that was assumed in the previous ICE-2 model of *Wu and Peltier* [1983]; clearly, the RSL data from Thores River cannot be reconciled with the thin ice sheet model suggested by *England* [1976a,b, 1983]. This controversy was discussed in greater detail by *Tushingham and Peltier* [1991] and will not be further elaborated here. The geological evidence may be reconciled by noting the possibility that delta E is a lacustrine feature. The floating tongue of Lorimer Glacier may have in the past thickened and become grounded, thus damming Thores River (J. Westgate, personal communication, 1987). The elevation of delta E would be an indicator of the level of the dammed lake and not of sea level. If delta E is a lacustrine feature, no marine shells would be associated with it, and in fact none were found.

Fig. 2. Thores River location map. The dots show the locations of the shell samples.
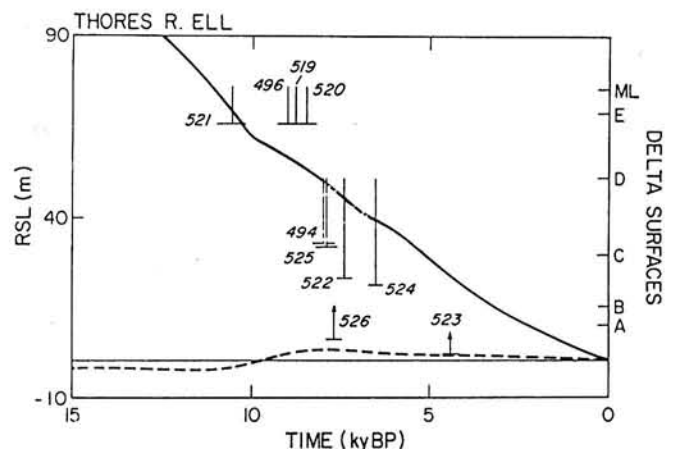

Fig. 3. Thores River relative sea level history. The solid line represents the ICE-3G predicted curve and the dashed line the ICE-2 predicted curve. The ages of the samples have been corrected to sidereal years using the curve presented in Figure 1a. Labels A-E locate the elevations of the delta surfaces and ML is the elevation of the marine limit.

The field work undertaken in Disraeli Fiord consisted of the collection of marine shells (all *Hiatella arctica*) from silt deposits located on the northern and southern flanks of the ancient delta, with additional shells collected from a smaller poorly preserved flight of deltas 5 km north of Thores delta (referred to here as Northern delta). The samples were radiocarbon dated using the accelerator mass spectrometer of the IsoTrace facility at the University of Toronto. The results of the radiocarbon analysis are presented in Table 1, with all results corrected for natural, preparation and sputtering fractionation to a base of $\delta^{13}C = 0\%$ and the errors representing the 68.3% confidence limits. Since it is very difficult to assign an exact sea level elevation to a sample elevation in this area, Table 1 displays both the actual sample elevation and an estimate of sea level. Fortunately, the highest samples (TO-496, 519, 520, and 521) are close to the marine limit in the area (about 75 m above sea level (asl)) and can therefore be considered good sea level indicators. These four whole bivalves of *H. arctica* were found insitu beside each other in the same deposit located on the north side of Northern delta. Whole bivalve is a term used to describe a sample which has both halves of its shell still connected, and thus one may infer that very minimal reworking of the shell by later processes has taken place. It is interesting to note that 2000 years separate the age of TO-521 from the other three samples. The sample may have been reworked, but it is difficult to envisage a reworking mechanism that would preserve the whole bivalve intact in the cobbly horizon in which the samples were found. Alternatively, the three younger samples may have become contaminated sometime during their history. Sample TO-522 consisted of two whole bivalves lying on the surface of a large silt deposit on the southern flank of Northern delta. The sample has probably been reworked, but since the shells were intact, the reworking is likely to have been minor. The silt deposit is located at the base of the best preserved delta in the flight of deltas. The elevation of this delta is 51 m on the basis of

which one may infer that it was formed at the same time as delta D at Thores delta.

Returning to Thores delta, sample TO-523 was a whole bivalve found washing out of delta A on the south side and can be considered to have been reworked. Sample TO-494 was a whole bivalve found in situ at the top of a small knob among the extensive silts on the southern flank of Thores delta, while sample TO-525 was a whole bivalve found nearly on the surface in its growth position, and as expected, the dates overlap. (Samples TO-494 and 496 are from *Lemmen* [1989].) Sample TO-524 was a whole bivalve found at a lower elevation on the surface of the same silt deposit. The above three samples (TO-494, 524, and 525) probably relate to the large well-preserved delta D which has an elevation of 51 m. The many single valves of sample TO-526 were collected from the silts located on the northern flank of Thores delta, even though it was likely they were extensively reworked. This reworking would explain the anomalously low elevation at which they were found. This sample illustrates very clearly the importance of being highly selective in collecting samples in the field. For shells, whole bivalves are the sample of choice because they imply that there has only been minimal reworking of the sample by processes such as erosion, downslope transportation, sea ice excavation, etc.

Figure 3 demonstrates how well, especially at the higher elevations, the RSL data from the Thores River area compares to the computed sea level from glacial isostatic rebound theory using the ICE-3G model of deglaciation. The younger samples were either deposited below sea level (TO-494, 522, 524, and 525) or extensively reworked (TO-523, and 526).

2.3. Compilation of the Global RSL Data Base

Our first step in compiling the new global data base of relative sea level histories began with inspection of three previous compilations (*Walcott* [1972], *Bloom* [1977], and W. Newman,

TABLE 1. Relative Sea Level Data From Thores River, Ellesmere Island, Northwest Territories, Canada

Laboratory Number	Uncorrected Age, Years B.P.	Sample Elevation, m asl	Estimated Sea Level, m asl	Latitude N	Longitude W
		South Thores River			
T0-523	4040±50	2	> 2	82°35'	72°47'
T0-524	4680±90	21	≤51	82°35'	72°50'
T0-525	7110±60	32	≤51	82°35'	72°50'
		North Thores River			
T0-526	6890±60	6	> 6	82°36'	72°47'
		Northern Delta			
T0-522	6460±60	23	≤51	82°38'	72°38'
T0-520	7800±60	64	≤75	82°39'	72°39
T0-519	7950±60	64	≤75	82°39'	72°39
T0-496	8150±80	64	≤75	82°39'	72°39
T0-521	10090±70	64	≤75	82°39'	72°39'

All samples are *Hiatella arctica* shells. Samples T0-494 and T0-496 are from *Lemmen* [1989].

(unpublished compilation copied to W. R. Peltier in 1984)), and from these the references to the original sources of individual radiocarbon controlled RSL records were extracted and the data presented in them examined. Many additional references not cited in these general references (in fact, the vast majority in our new data base) were also examined and RSL data from them extracted, eventually leading to the compilation of the 392 RSL sites that constitute the new global collection. These sites have been somewhat arbitrarily grouped into the following six geographic regions to aid in subsequent analysis: (1) Arctic Canada and Greenland, (2) northern Europe including Great Britain, Iceland, Spitsbergen, and Franz Joseph Land, (3) the east coast of North America, (4) southern Europe and the Mediterranean Sea, (5) the Atlantic, Indian, and Southern oceans, and finally (6) the Pacific Ocean. This arbitrary grouping roughly divides the globe into two ice-covered regions (1 and 2), two ice-marginal regions (3 and 4), and two far-field areas (5 and 6). In the bibliography of Appendix A (on microfiche) is listed each of the references used in the compilation of this data base and the site to which the RSL data from them applies. The individual sample elevations for these ancient sea levels and their associated uncorrected radiocarbon ages are provided in Appendix B (on microfiche). The excellent global distribution provided by this extensive data base is illustrated in Figure 4.

When dealing with such a large data base obtained from numerous different primary sources, it was obviously necessary to take steps to ensure consistency and homogeneity of the compilation. To this end, elevations were always taken in meters above high tide and ages in radiocarbon years before present. If as in some cases RSL data were scattered over a small area (e.g., Keewatin), the geographical center of the region was chosen to define the site location. In a few locations the quantity of data was so large that only elevations at thousand-year intervals were recorded (e.g., Cape Storm). It was also necessary to be consistent in handling the uncertainties in the sample ages and elevations. Upon review of many volumes of *Radiocarbon* and *Litherland et al.* [1980], it was determined that the average accuracy of conventional radiocarbon dating is usually ±3%. Accelerator mass spectrometry is often used to an accuracy of approximately ±0.3% [*Beukens*, 1984], but as yet only a few RSL samples have been dated by this method. Since some ages are based on marine samples and such samples respond to the flux of ^{14}C into the oceans, the radiocarbon dates should be corrected by using a marine ^{14}C correction curve (a damped version of the atmospheric ^{14}C correction curve presented in Figure 1b). To incorporate this effect and uncertainties in the atmospheric correction curve itself, the uncertainty in the ages has been increased to ±4% with a minimum uncertainty of ±200 years. Uncertainty in the elevation may be due to the direct error in measuring the altitude of the sample or the position of high tide or, more importantly, the potential uncertainty in geological interpretation. From the 35 RSL sites listed by *Walcott* [1972], we estimate the range of uncertainty in elevation to be ±15%, with a minimum error of ±1 m assigned due to wave action and instrument error. If the original reference cited larger uncertainties in either the age or the elevation, those values have been employed. The uncertainty assigned to the elevation of the sample also includes the effect of tectonic uplift or subsidence. At some sites, such as Crete [*Pirazzoli et al.*, 1982] and Taiwan [*Taira*, 1975], the tectonic effects were so obvious that the RSL data from these sites were omitted from the data base, but at other sites the magnitude of tectonic elevation changes were smaller and thus could be incorporated in the assigned uncertainties in elevations. To minimize these uncertainties, extreme care must be taken in selecting samples and inferring associated sea levels. It is now possible and preferable, with the advent of accelerator mass spectrometry, to date individual samples from a single deposit instead of estimating the age of an aggregate sample. This method will immediately allow anomalous samples to be discounted from the average age of the deposit as mentioned previously.

It is hoped that the global RSL data base that we have compiled according to the above described procedures will help to focus attention on regions where more work is needed to establish a well-defined sea level curve and to provide a comprehensive reference for researchers in widely diverse fields of study.

3. VERIFICATION OF ICE-3G USING FAR-FIELD RSL DATA

In the construction of the deglaciation chronology ICE-3G, the RSL histories from 192 ice-covered sites were employed to constrain the thickness of the ice sheets (as described by *Tushingham and Peltier* [1991]). The RSL histories from the remaining 200 sites (generally located far from any ice sheet and denoted by the triangles on Figure 4) can be used to verify the accuracy of the ICE-3G model. Figure 5 displays a sample of comparisons of observed RSL histories and predicted RSL curves for the new ICE-3G model and the old ICE-2 model (as compiled by *Wu and Peltier* [1983]). For this initial set of comparisons the conventional calibration curve of Figure 1a has been used to correct ^{14}C dates to sidereal years. The Wairau Valley (New
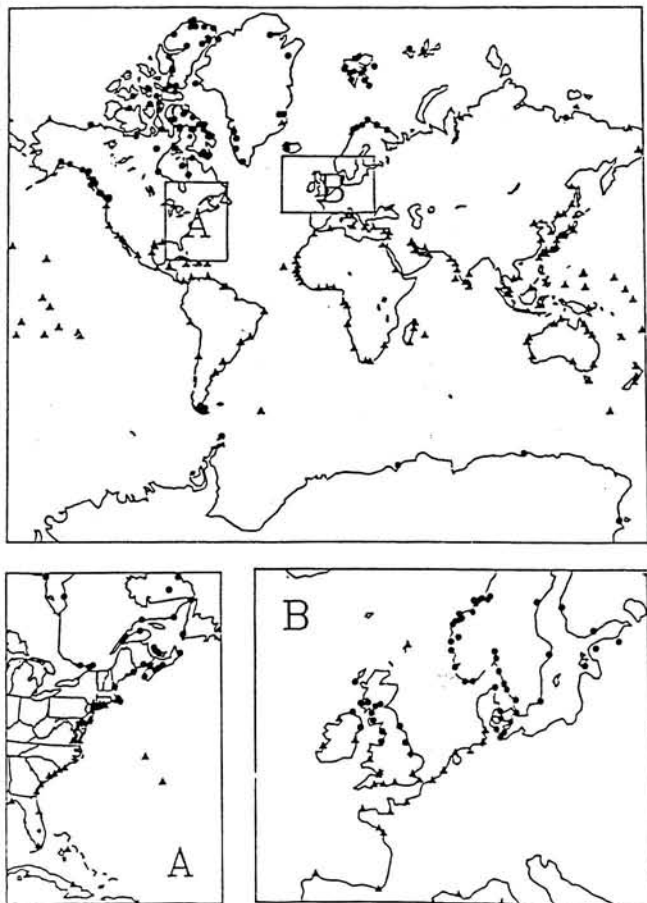

Fig. 4. Complete RSL site location map. For eastern North America and Europe refer to enlargements A and B, respectively. The dots represent sites employed in constructing ICE-3G and the triangles sites used in verifying ICE-3G.
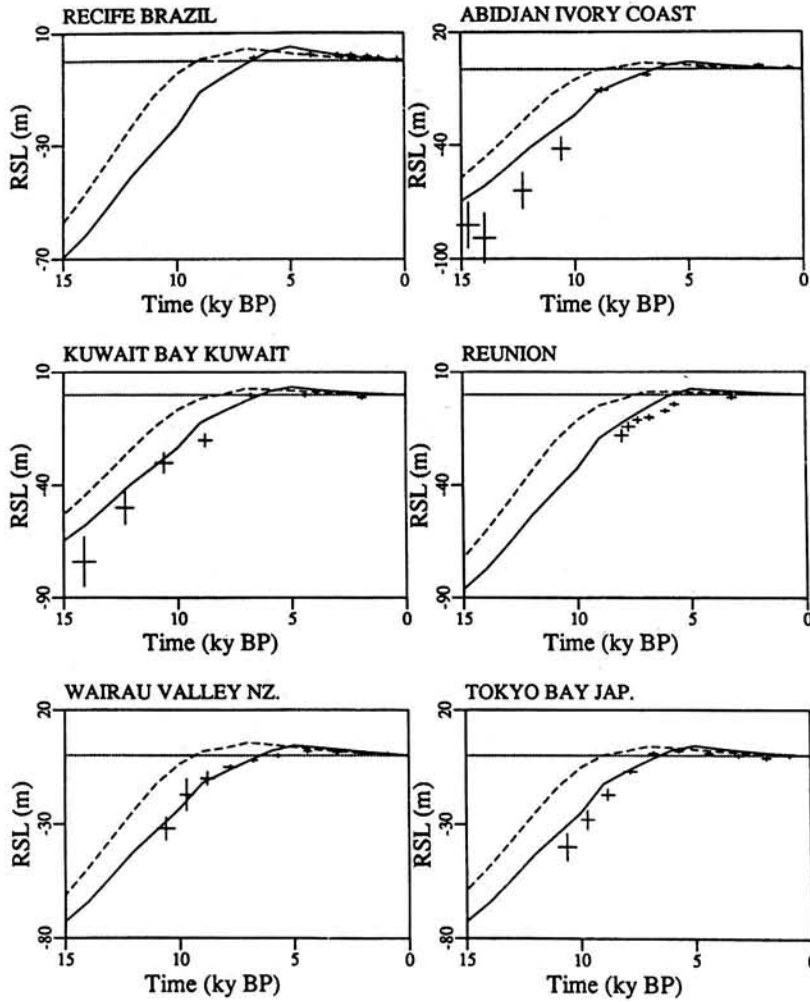
Fig. 5. RSL predictions for far-field sites. The differences between ICE-2 and ICE-3G predictions are mostly due to the delay in Antarctic melting.

Zealand) site was in fact employed in the construction of ICE-3G to control the timing of the deglaciation of Antarctica following the argument of *Peltier* [1988], but the predictions at the other five sites (which were not used to construct ICE-3G) also agree reasonably well with the observed RSL histories, particularly during the last 10,000 years. The older RSL data from several of these sites and all the data from the Reunion site could be taken to indicate that a further delay of the melting of Antarctic ice (of say 500 years) was required. However, if such a delay were incorporated into the ICE-3G model, the predicted RSL curve would not agree well with the more recent data at these sites (except Reunion) and many other sites, as we shall see later in this section. In fact, the rather large errors at Kuwait, Abidjan, and Tokyo Bay are entirely a consequence of our having employed the erroneous ^{14}C calibration of Figure 1a rather than the more recently derived and evidently superior relationship provided by the analysis of *Bard et al.* [1990] that we presented in Figure 1b. On Figure 6, for comparison purposes, we show a set of six further comparisons of theory and observations at far-field sites where both the uncorrected and the U-Th corrected ages are employed to plot the data (solid and dashed error bars respectively). At all sites but eastern Panama the properly corrected data fit the theoretical prediction, whereas the uncorrected data do not. The most important of the comparisons presented on Figure 6, however, is

that for Barbados that is based on the U-Th dating by *Bard et al.* [1990] of the coral-based sea level record of *Fairbanks* [1989] since this record extends back to 22,000 sidereal years before present. Back to 18 kyr B.P. it is clear that the theory fits the data very well. However, it is clear that these new data put the onset of deglaciation nearer to 22 kyr B.P., and suggest that the ICE-3G model is still somewhat deficient in total ice volume at glacial maximum, by an amount near 15 m eustatic, or about 10% of the volume at maximum in ICE-3G. This small remaining discrepency will require correction in the next stage of refinement of the deglacition model.

Tushingham and Peltier [1991], performed a "variance" reduction calculation to estimate numerically the quality of the agreement between predictions and observations. A global measure of the variance σ was computed using

$$\sigma = \frac{1}{N} \sqrt{\sum_{i=1}^{N} (H_i^p(t) - H_i^o(t))^2} \ ,$$

where $H_i^p(t)$ and $H_i^o(t)$ are the predicted and observed sea level heights at time t, respectively, and N is the number of RSL data points in the global data set. The uncertainty in the observed age (Δt) was incorporated into the variance by varying the time from
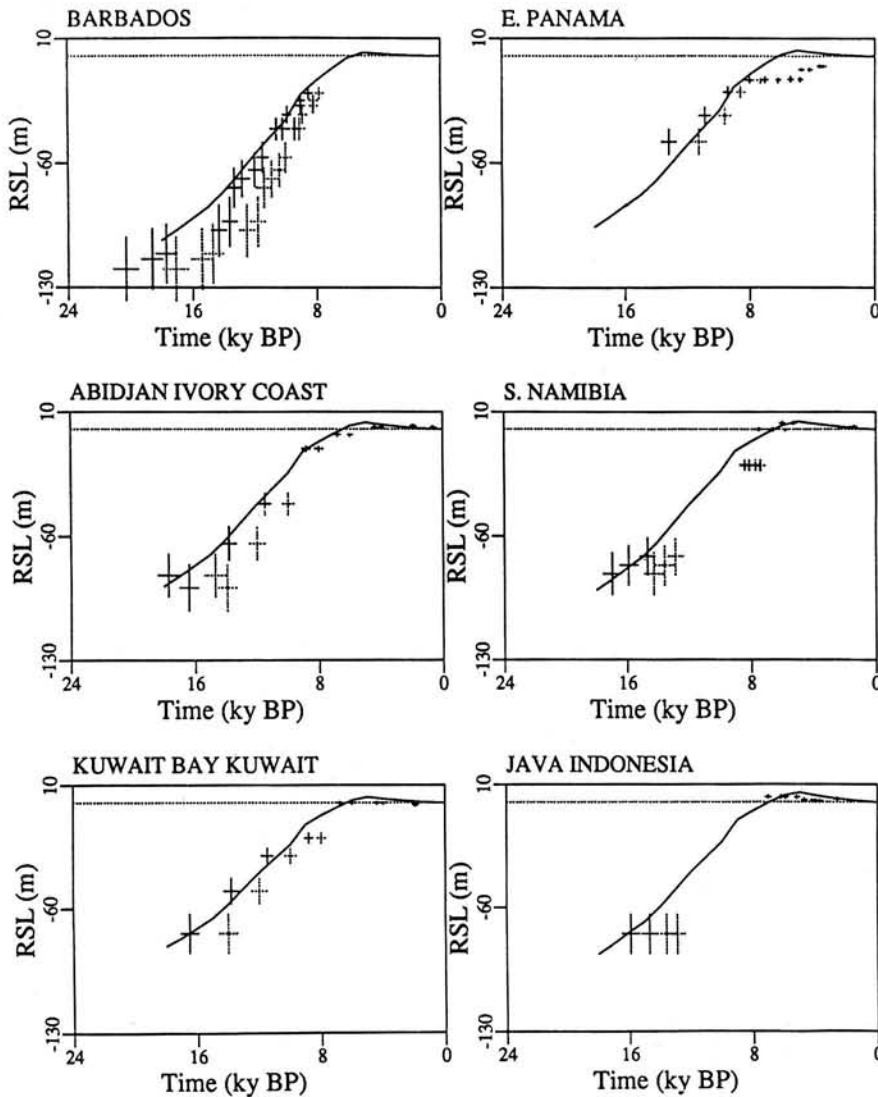
Fig. 6. RSL predictions with the ICE-3G model at a number of far-field sites plotted against the raw data (dotted error bars) and the data plotted using the ^{14}C calibration cure of *Bard et al.* [1990].

t - Δt to t + Δt and finding the minimum value of the height difference. The uncertainty in the observed height $\Delta H_i^o(t)$ was employed to determine the minimum variance possible given the uncertainty in the data set by using

$$\sigma_{min} = \frac{1}{N} \sqrt{\sum_{i=1}^{N} (2\Delta H_i^o(t))^2} .$$

The factor of 2 incorporates the range of uncertainty between $-\Delta H_i^o(t)$ and $+\Delta H_i^o(t)$. Table 2 gives a summary of the variance calculation for the entire far-field data set by region as well as globally. (The Wairau Valley site is not included in this far-field data set as it was employed in the construction of ICE-3G.) In the northern Europe region the English and Irish RSL data overwhelmingly prefer the ICE-3G model over the old ICE-2 model of *Wu and Peltier* [1983], due mostly to the reconstruction of the Scottish Ice Sheet. The southern Europe and Atlantic, Indian and southern oceans regions also prefer the ICE-3G model. Upon examining the RSL data in the region of eastern North America, it appears that most of the sites north of the entrance to

Chesapeake Bay do in fact prefer ICE-3G but south of the entrance ICE-2 is preferred. The problem in this region is most probably due to the assumption of a lithospheric thickness of 120 km, but this assumption will be tested in section 4 (and will be found to be unsatisfactory for this region). In the Pacific Ocean region, the ICE-2 model is slightly preferred to the ICE-3 model when the ^{14}C correction is made using the erroneous calibration of Figure 1a. This slight preference is reversed when the more accurate calibration curve of Figure 1b is employed. The differences in the predictions of the two models during the last 5000 years are minor, whereas the differences in earlier predictions are quite large; therefore the older RSL data are more useful in constraining the deglaciation history than are the younger RSL data. Since the older RSL data prefer the ICE-3G model, Antarctic melting can be inferred to be delayed from the ice sheets of the northern hemisphere as suggested on the same basis in Peltier (1988). Overall the significant improvements in the Southern European and Atlantic, Indian and southern oceans regions along with the slight improvement in the quality of agreement in the Pacific Ocean region, demonstrate a global preference of the data for the ICE-3G model.

TABLE 2. Variance Statistics for RSL Sites Used to Verify ICE-3

Region	Number of Sites	Number of Data	Variance		
			ICE-2	ICE-3	Minimum
Arctic Canada and Greenland	0	0	0.00	0.00	0.00
Northern Europe	13	46	1.25	0.48	0.68
Eastern North America	34	175	0.75	0.90	0.68
Southern Europe	24	102	0.82	0.62	0.49
Atlantic, Indian and Southern Oceans	65	254	0.59	0.34	0.35
Pacific Ocean	64	293	0.46	0.51	0.21
Global	200	870	0.30	0.28	0.20

Sites which are ICE-2 Preferred = 51 neutral = 64 ICE-3 preferred = 85. ICE-2 fits 45.0% of the sites within the minimum variance and 74.5% within twice the minimum variance. ICE-3 fits 53.5% of the sites within the minimum variance and 81.5% within twice the minimum variance.

4. SENSITIVITY OF RSL PREDICTIONS TO VARIATIONS IN THE RADIAL VISCOELASTIC STRUCTURE

To completely specify the viscoelastic Earth structure, two basic classes of physical property must be described as functions of radius, namely the elastic/density structure and the viscosity variation. The elastic/density structure employed in the present work is the seismically determined 1066B model of *Gilbert and Dziewonski* [1975]. Using a linearly viscoelastic Maxwell representation of the rheology of the mantle, *Peltier et al.* [1986] demonstrated that the Earth's radial response to an applied load was relatively insensitive to realistic changes in the elastic/density structure but very sensitive to changes in the radial viscosity profile. The model of the radial viscosity variation is here taken to be parameterized by the contrast in viscosity across the 670-km seismic discontinuity and the thickness of the lithosphere.

The "standard" Earth model that was employed for the purpose of constructing ICE-3G and for the analyses reported above has an upper mantle viscosity of 10^{21} Pa s, a lower mantle viscosity of 2 $\times 10^{21}$ Pa s, and a lithospheric thickness of 120 km. The viscosity values for the upper and lower mantle are reasonably well constrained by simultaneous agreement of several types of geophysical observations [*Peltier et al.*, 1986], but the lithospheric thickness is less certain and known on a priori grounds to be an Earth property that is strongly heterogeneous laterally. Here we shall illustrate the sensitivity of the ICE-3G model to changes in the Earth model by (1) maintaining the standard viscosity contrast and varying the lithospheric thickness, (2) maintaining the standard lithospheric thickness and varying the viscosity contrast, (3) including a low-viscosity zone, and (4) investigating the influence of using a different elastic model.

4.1. *Lithospheric Thickness*

With the upper and lower mantle viscosities set at 10^{21} Pa s, and 2 $\times 10^{21}$ Pa s, respectively, the lithospheric thickness was varied through the sequence of values 71, 120, 196, and 245 km. A number of interesting characteristics of the variations of relative

sea level associated with changes in lithospheric thickness are illustrated in Figure 7. At Wairau Valley and all such far-field sites, the response is relatively insensitive to changes in lithospheric thickness as RSL histories at such sites are most strongly dependent on the redistribution of meltwater. On the margins of large continents in the far field, however, the sensitivity can be more pronounced [*Peltier*, 1988]. In the central region of the huge Laurentide Ice Sheet (e.g., Churchill), the response is also insensitive to changes in lithospheric thickness; however, this is due to a different mechanism than that operating in the far field. Due to the great mass and horizontal extent of this ice sheet, the central response is predominately dependent on deep-earth structure rather than shallow-earth structure, and as we shall see in section 4.2 this region is therefore far more sensitive to lower mantle viscosity changes. Sites which were covered by smaller ice sheets (e.g., Stockholm and Edgeoya) and regions closer to the margin of the Laurentide Ice Sheet (e.g., Rimouski) are very sensitive to changes in lithospheric thickness. The forebulge region of the Laurentide Ice Sheet is also quite sensitive to these changes (e.g., at Chester River). Table 3 presents the variance calculation for sites inside or very nearly inside the ice margins of ICE-3G. Since all the interior sites were used in the construction of ICE-3G, it is not surprising that the global variance and the variance for four of the six regions prefer a value of 120 km for the thickness of the lithosphere. The very large variance for all lithospheric models in the Atlantic, Indian, and southern oceans regions is due to the very poor fit at one Antarctic site, namely McMurdo Sound, which has 8 of the 16 data points for this region. The two West German sites in the southern Europe region, which are both ice-marginal sites, prefer the thickest lithospheric model, and as we shall see this may be significant.

The variance calculation for sites outside of the ice margin is summarized in Table 4. The very small difference between variance values of the various lithospheric models for both the Atlantic, Indian, and southern oceans region and the Pacific Ocean region confirm the insensitivity of the radial response to changes in the thickness of the lithosphere. The English and Irish RSL data
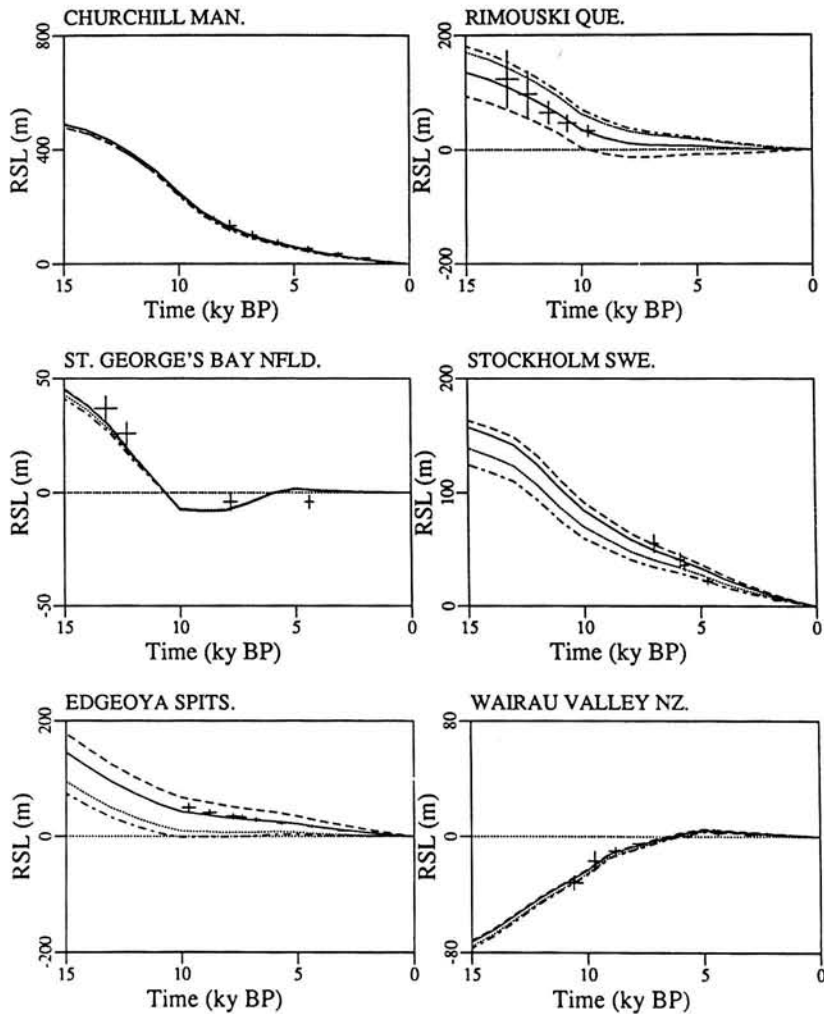
Fig. 7. RSL predictions for various lithospheric thickness. Note the insensitivity of the response at ice-centred (Churchill) and far-field (Wairau Valley) sites. The lines are as follows: dashed 71 km; solid, 120 km; dotted, 196 km; and dash-dotted 245 km.

TABLE 3. Variance Statistics for Various Lithospheric Thicknesses

Region	Number of Sites	Number of Data	Variance at Lithospheric Thickness, km				
			71	120	196	245	Minimum
Arctic Canada and Greenland	69	365	0.89	0.75	0.99	1.19	1.09
Northern Europe	73	397	0.75	0.61	0.94	1.12	0.59
Eastern North America	25	152	1.65	1.32	1.42	1.58	1.71
Southern Europe	2	11	2.63	1.93	1.11	1.06	1.41
Atlantic, Indian, and Southern Oceans	5	16	2.96	3.63	4.51	5.09	0.73
Pacific Ocean	17	69	4.05	3.12	3.22	3.56	1.42
Global	191	1010	0.58	0.47	0.60	0.71	0.53

For RSL sites inside the ICE-3G Margin.

TABLE 4. Variance Statistics for Various Lithospheric Thicknesses

| Region	Number of Sites	Number of Data	Variance at Lithospheric Thickness, km				
			71	120	196	245	Minimum
Arctic Canada and Greenland	0	0	0.00	0.00	0.00	0.00	0.00
Northern Europe	13	46	0.57	0.48	0.51	0.54	0.68
Eastern North America	34	175	0.97	0.90	0.81	0.75	0.68
Southern Europe	24	102	0.68	0.62	0.55	0.53	0.49
Atlantic, Indian, and Southern Oceans	65	254	0.37	0.34	0.32	0.31	0.35
Pacific Ocean	65	303	0.52	0.49	0.51	0.50	0.21
Global	201	880	0.30	0.28	0.26	0.25	0.20

For RSL sites outside the ICE-3G Margin.
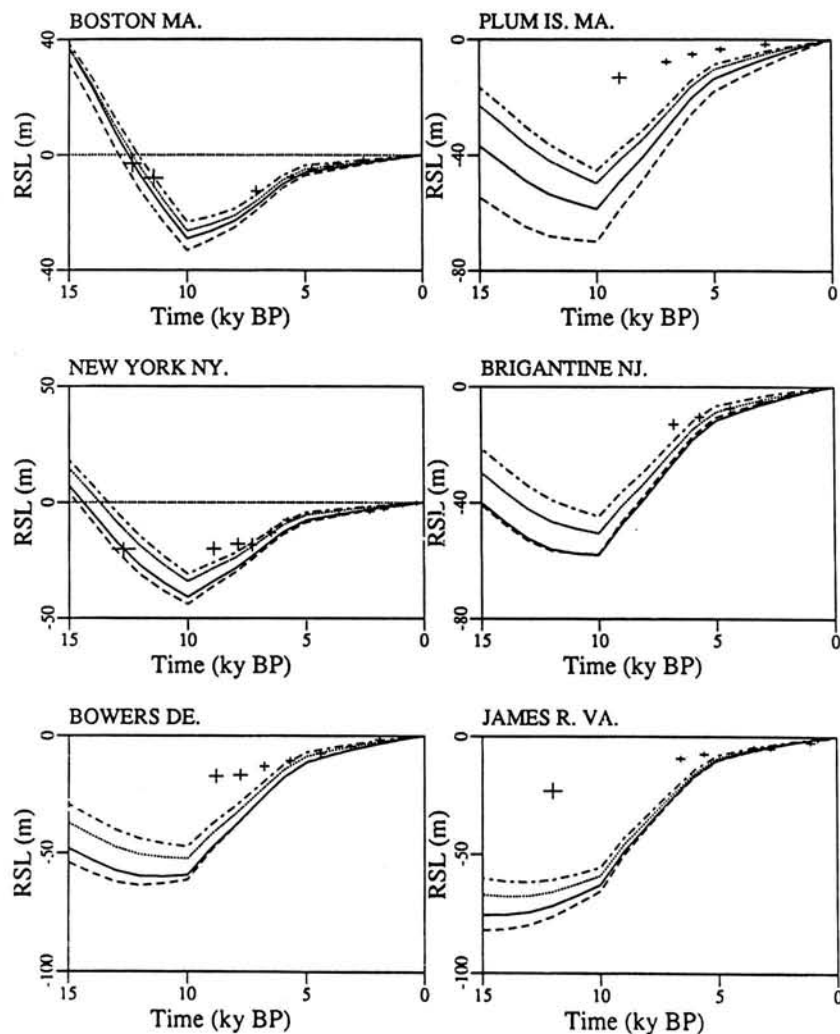
Fig. 8. RSL predictions along the U.S. east coast for various lithospheric thicknesses. The RSL data have a preference for a thick lithosphere.

from the northern Europe region are seen to prefer a lithospheric thickness of 120 km, but all models produce variances which are less than the minimum and thus all are potentially acceptable. Since ice central and far-field sites are relatively insensitive to changes in lithospheric thickness, the regions of most interest are those which are located near the ice margin and both the eastern North America and the southern Europe regions show significant preference for the thickest lithospheric model. A sample of six RSL histories from the eastern North America region, all of which prefer lithospheric thicknesses greater than the standard 120 km, are displayed in Figure 8. This weak preference for a lithospheric thickness of about 245 km, particularly in the eastern North American region, agrees with previous estimates based on the same data [Peltier, 1986, 1988]. Inspection of this information does, however, demonstrate that the fits to the data for ages in excess of 5 kyr at many sites along the U.S. east coast remains rather poor, with the data showing much less submergence than is predicted by the theory. This may be due in large part to the severe problems encountered in accurately interpreting the observations from this "drowned" coast. Until we understand these data better than we do at present, we can have no particular confidence in our inference of lithospheric thickness from them.

4.2. *Viscosity Contrast Between Upper and Lower Mantle*

With the lithospheric thickness set at 120 km and the upper mantle viscosity set at 10^{21} Pa s, the lower mantle viscosity was varied through the sequence 10^{21}, 2×10^{21} (the standard model), 4×10^{21}, 10^{22}, and 10^{24} Pa s. As shown by *Peltier et al.* [1986], increases in the lower mantle viscosity above 10^{24} Pa s do not further affect the radial response as the lower mantle is then behaving as essentially rigid with respect to the upper mantle. Figure 9 displays the responses delivered by these various viscosity models at a sample of six RSL sites. As expected, the response in the far field (e.g., Tokyo Bay) was found to be essentially insensitive to any variation in lower mantle viscosity, as was also found to be the case for many sites with respect to variations in lithospheric thickness. In the central regions of major ice sheets (Richmond Gulf, Keewatin, and Stockholm) the response is very dependent on viscosity contrast within the mantle as shown in many previous studies [e.g., *Peltier and Andrews*, 1976]. The total uplift and the steepness of the RSL curves both decrease as the lower mantle viscosity increases. Obviously, the ice model would have to be substantially thickened for the responses of the higher viscosity contrast models to fit the RSL data at the
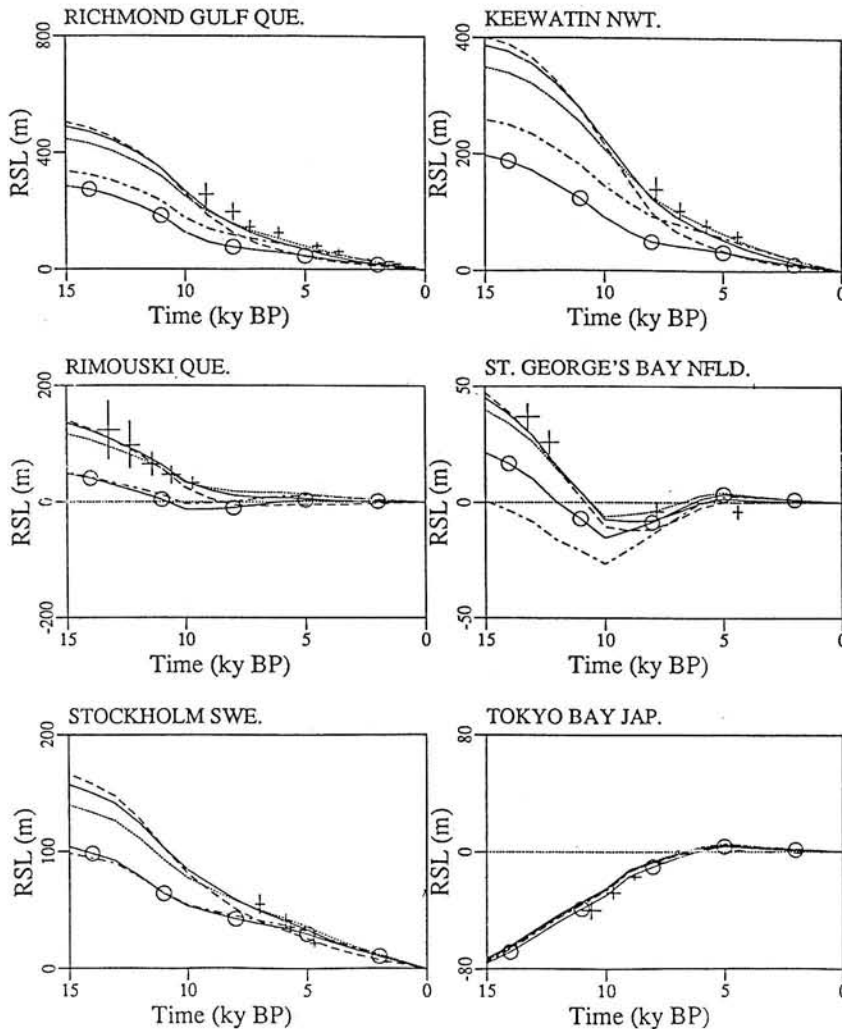

Fig. 9. RSL predictions for various mantle viscosity contrasts. Note the insensitivity of the response at the far-field (Tokyo Bay) site. The lines are as follows: dashed 1:1 contrast; solid, 1:2; dotted, 1:4; dash-dotted, 1:10; and solid with circles, 1:1000.

central sites, but this in turn would mean an excess of meltwater entering the oceans and the far-field data would not agree with this much larger predicted sea level rise. Over Richmond Gulf, for example, the thickness of ice would have to be increased from its ICE-3G value of approximately 3200 m to an excessive value of over 5500 m! In the ice marginal region (St. George's Bay and Rimouski), the response is much more complex. As demonstrated by *Peltier et al.* [1986], the position, extent, and migration characteristics of the forebulge are very sensitive to changes in viscosity contrast, and these are confirmed here. The substantial lateral migration of the inner margin of the forebulge that is predicted when lower viscosity contrast models are employed ceases as the viscosity contrast is increased. Furthermore, the areal extent of the forebulge is decreased as the viscosity contrast is increased [*Pelter et al.*, 1986]. The complex sensitivity of the forebulge is illustrated in the series of RSL curves from sites along the eastern North American coast shown in Figure 10. Note that the uniform viscosity model predicts a raised beach at the Everglades site and other sites from South Carolina to Texas, but these beaches are not observed in the field. Furthermore, the RSL data at the ice-marginal sites (Boston and New York) strongly reject the two models with highest lower mantle viscosity ($\geq 10^{22}$ Pa s).

Tables 5 and 6 present the results of the variance calculations undertaken for the various viscosity models inside and outside the ice margin, respectively. Within the ice margin, not surprisingly, the standard model is somewhat preferred, although the two nearest models 10^{21} and 4×10^{21} Pa s have variance values almost as small. The two exceptions to this preference are the McMurdo Sound, Antarctica, site with RSL data which prefer the 10^{22} Pa s model and the Alaska and British Columbian data which marginally prefer the 4×10^{21} Pa s model. Note the variance for the southern Europe region (based on two West German sites) is smaller for the 10^{24} Pa s model than it is for the 10^{22} Pa s model but still much larger than the low contrast values. As shown in Table 5, the x 10 contrast model is preferred over the standard by sites in the Atlantic, Indian, and southern oceans region but eastern North America, southern Europe, and Pacific Ocean data all prefer the same modest viscosity contrast model that was employed to refine the deglaciation history at interior sites. High viscosity contrast models can also be discounted on the basis of the following two additional reasons: (1) the complex shapes of certain ice-marginal RSL curves implied by the RSL data cannot be reproduced by either of the high viscosity models (French River, Boston, and New York; refer to Figure 10), and most importantly (2) the high viscosity model is not self-consistent; that is to say, the additional amount of ice that would be required in ice central sites to model correctly the radial response (e.g., Richmond Gulf) would mean that the predicted far-field response would no longer agree with the observed RSL data in these regions (e.g., Barbados,
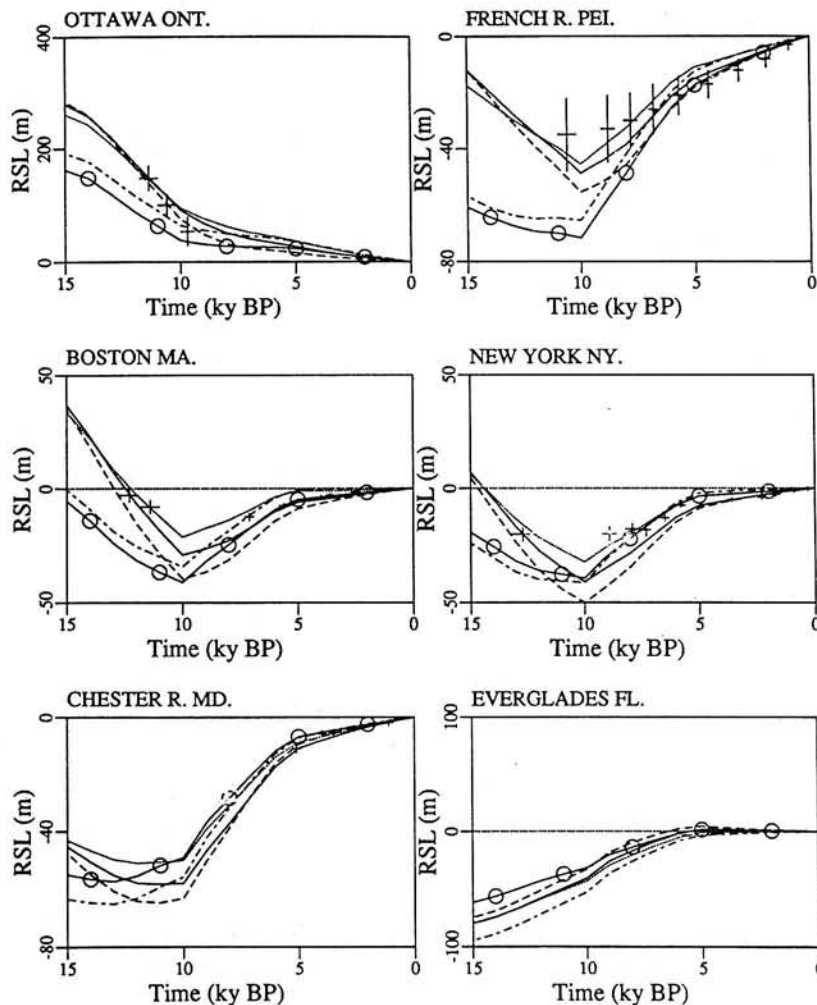

Fig. 10. RSL predictions along the U.S. east coast for various viscosity contrasts. Note the complex sensitivity in the forebulge region, particularly at the Boston, New York, and Chester River locations. (Refer to Figure 9 for the legend.)

TABLE 5. Variance Statistics for Various Mantle Viscosity Contrasts

Region	Number of Sites	Number of Data	Variance at Mantle Viscosity Contrasts (UM:LM)					
			1:1	1:2	1:4	1:10	1:1000	Minimum
Arctic Canada and Greenland	69	365	0.94	0.75	0.83	1.44	2.13	1.09
Northern Europe	73	397	0.71	0.61	0.70	1.13	1.18	0.59
Eastern North America	25	152	1.50	1.32	1.36	2.54	2.82	1.71
Southern Europe	2	11	1.96	1.93	2.42	3.52	2.68	1.41
Atlantic, Indian, and Southern Oceans	5	16	3.07	3.63	3.21	1.43	1.91	0.73
Pacific Ocean	17	69	3.37	3.12	3.03	4.17	3.63	1.42
Global	191	1010	0.55	0.47	0.50	0.84	1.02	0.53

For RSL sites inside the ICE-3G Margin.

TABLE 6. Variance Statistics for Various Mantle Viscosity Contrasts

Region	Number of Sites	Number of Data	Variance at Mantle Viscosity Contrasts (UM:LM)					
			1:1	1:2	1:4	1:10	1:1000	Minimum
Arctic Canada and Greenland	0	0	.00	.00	.00	.00	.00	.00
Northern Europe	13	46	.52	.48	.55	.83	.59	.68
Eastern North America	34	175	.92	.90	.80	1.01	.61	.68
Southern Europe	24	102	.68	.62	.63	.73	.72	.49
Atlantic, Indian, and Southern Oceans	65	254	.33	.34	.34	.34	.29	.35
Pacific Ocean	65	303	.45	.49	.52	.62	.42	.21
Global	201	880	0.27	0.28	0.27	0.32	.22	.20

For RSL sites outside the ICE-3G Margin.

see Figure 6). Upon review of the balance of Table 5, it will be observed that the preference of the data is not strong between the three lowest viscosity contrast models. Since the uniform model has been discounted due to its prediction of nonexistent raised beaches in Florida, the viscosity contrast between the upper and the lower mantle can be concluded to lie between a factor of 2 and a factor of 4. It should be noted, however, that these analyses have all been predicated upon the assumption that the upper mantle viscosity is very near 10^{21} Pa s, a number that is very strongly constrained by the Fennoscandia data and therefore not amenable to variation on a priori grounds if we confine our attention to models in which the lateral heterogeneity of viscosity is assumed small.

4.3. The Influence of a Sublithosphere Low-Viscosity Zone

A model with a low-viscosity zone beneath the lithosphere was introduced in the glacial isostatic rebound analysis in an attempt to resolve a problem existing with the ICE-3G predictions along the Greenland and central Norwegian coasts (which will be discussed below). The low-viscosity zone (LVZ) model was identical to the standard model except in a region between depths of 120 and 220 km which corresponds to the seismically determined low-velocity zone found beneath mid-ocean basins [cf. *Dziewonski and Anderson*, 1981]. The viscosity in this region was set at 10^{20} Pa s. As can be seen by inspection of the comparisons presented in Figure 11, ice-central sites (Churchill) are essentially insensitive to the presence of a low-viscosity zone, because they are dominated by long-wavelength dynamics, but ice-marginal sites (St. George's Bay and Kvalvika) and sites once under small ice caps (Stadarholskirkja and Bahia Gente Grande) are very sensitive to such structure. In the far-field (Tokyo Bay) the LVZ model usually predicts higher raised beaches, which are not observed in the data. The variance calculation results for the LVZ model as presented in Tables 7 and 8 display a very marked preference for the standard model. The exceptions to this overwhelming preference are the poorly fitting McMurdo Sound site and the southern Europe region both inside and outside the ice-margin, although the margin of preference is small. Figure 12 presents a sample of six of these Southern European sites and demonstrates that sites located along the North Sea and English Channel coasts
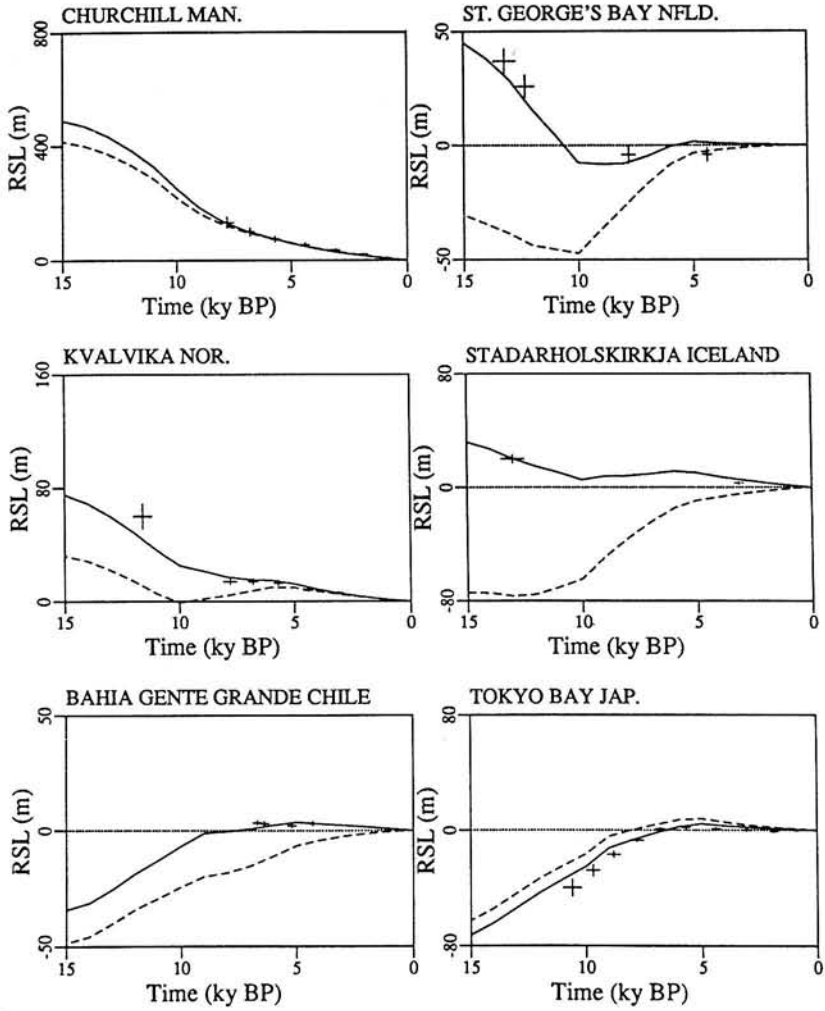
Fig. 11. RSL predictions for the low-viscosity zone model. The lines are as follows: dashed, low-viscosity zone model; solid, standard model.

TABLE 7. Variance Statistics for the Low-Viscosity Model

Region	Number of Sites	Number of Data	Variance		
			LVZ	STD	Minimum
Arctic Canada and Greenland	69	365	1.35	0.75	1.09
Northern Europe	73	397	1.79	0.61	0.59
Eastern North America	25	152	3.47	1.32	1.71
Southern Europe	2	16	3.05	3.63	0.73
Atlantic, Indian, and Southern Oceans	5	16	3.05	3.63	0.73
Pacific Ocean	17	69	5.26	3.12	1.43
Global	191	1010	1.07	0.47	0.53

For RSL sites inside the ICE-3G Margin. Sites which are LVZ preferred = 14 neutral = 40 STD preferred = 137. LVZ fits 23.6% of the sites within the minimum variance and 46.1% within twice the minimum variance. STD fits 54.5% of the sites within the minimum variance and 80.6% within twice the minimum variance.
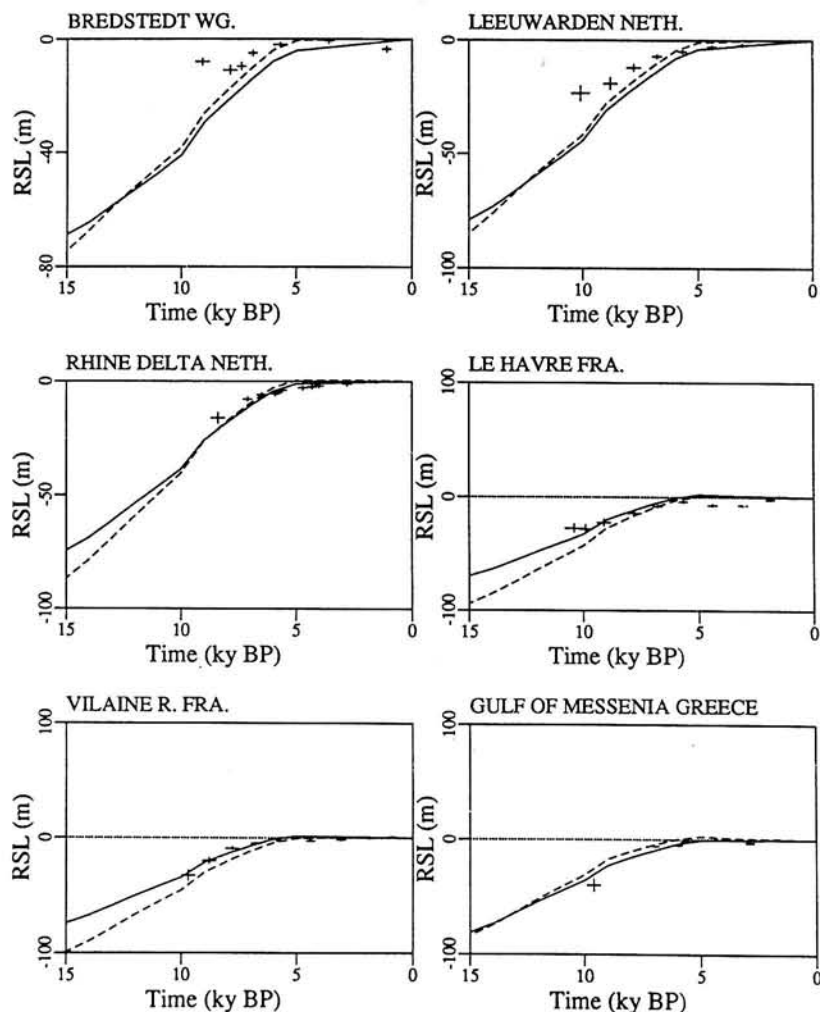
Fig. 12. RSL predictions for southern European sites for the low-viscosity zone model. Note the preference for the low-viscosity zone model along the North Sea and English Channel coasts.

TABLE 8. Variance Statistics for the Low-Viscosity Zone Model

Region	Number of Sites	Number of Data	Variance		
			LVZ	STD	Minimum
Arctic Canada and Greenland	0	0	0.00	0.00	0.00
Northern Europe	13	46	1.45	0.48	0.68
Eastern North America	34	175	2.37	0.90	0.68
Southern Europe	24	102	0.52	0.62	0.49
Atlantic, Indian, and Southern Oceans	65	254	0.57	0.34	0.35
Pacific Ocean	65	303	1.03	0.49	0.21
Global	201	880	0.62	0.28	0.20

For RSL sites outside the ICE-3G Margin. Sites which are LVZ preferred = 29 neutral = 39 STD preferred = 133. LVZ fits 25.4% of the sites within the minimum variance and 53.2% within twice the minimum variance. STD fits 53.7% of the sites within the minimum variance and 81.6% within twice the minimum variance.

(Bredstedt, Leeuwarden, and Le Havre) slightly prefer the LVZ model while the Atlantic and Mediterranean sites (Vilaine River and Gulf of Messenia) do not. The preference at North American sites is, however, decidedly in favor of the standard model, as shown in Figure 13. Even the shape of the RSL curve predicted using the LVZ model is very different from that characteristic of the RSL data.

Since the presence of a low-viscosity zone obviously has important geophysical implications, it will be useful to illustrate the differences between the relaxation spectra of the standard and LVZ models. Figure 14 compares the relaxation spectra for the standard and LVZ models, while such diagrams for the other models are presented elsewhere [e.g., *Peltier et al.*, 1986]. Note that time has been nondimensionalized with a characteristic time of 10^3 years so that $\log_{10}(-s) = -1$ corresponds to a relaxation time s^{-1} of 10^4 years. Employing the nomenclature of *Peltier* [1976], MO, LO, and CO are the family of fundamental modes of the mantle, lithosphere, and core, respectively, and the higher modes are similarly labelled as M1, M2, and C1. The mantle modes MO, M1, and M2 exist due to the density jumps across the free outer surface of the model, across the 670-km boundary and across the 420-km boundary, while the CO and C1 modes exist due to the density jump across the core-mantle boundary and across the inner-outer core boundary. The LO mode exists due to the very large viscosity contrast between the lithosphere and the mantle. The many transition modes, associated with the transition from elastic to Newtonian viscous behavior [*Peltier*, 1976], are not shown in Figure 14 because their amplitudes are negligibly small. According to Figure 14 the MO branch, with a response time of the order of 10^3 years, dominates the response especially for the higher modes ($\ell > 10$). For modes with lower spherical harmonic degree ($\ell < 10$) the MO branch still has the largest modal amplitudes, but the M1, LO, and CO branches also have significant strengths. The very long response times for the M2 and C1 branches (10^6-10^8 years) have little effect on the response because of their small modal amplitudes. The introduction of a low-viscosity zone just beneath the lithosphere generally does not cause any changes in the modes derived from density discontinuities that occur beneath the low-viscosity zone (i.e. CO, C1, M1, and M2). However, above this zone, the shape of the MO and LO branches are now quite different as the response times for these two branches are shorter (particularly for the LO branch). This is as expected since the lower viscosity of the material in the zone would result in a more rapid return to an equilibrium state than in the absence of such a feature. The modal amplitudes are, however, only modestly changed from their standard values.
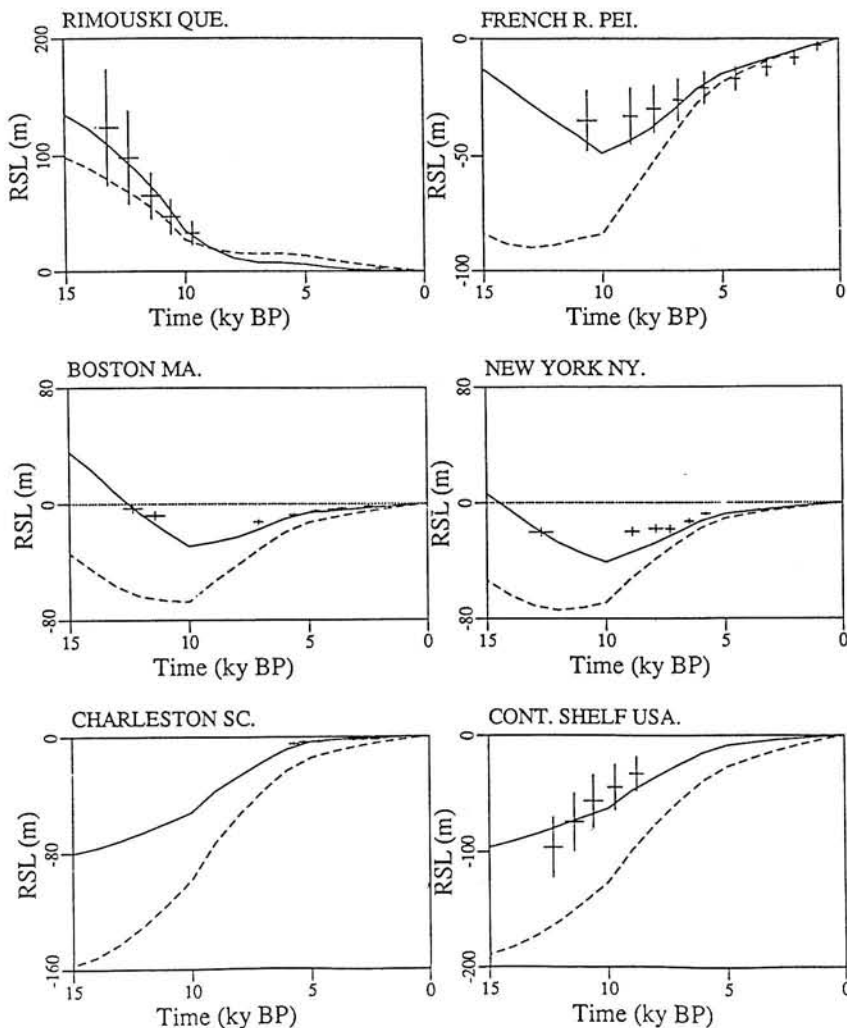

Fig. 13. RSL predictions for eastern North American sites for the low-viscosity zone model. Note the quite different RSL curves for the low-viscosity zone model.

4.4. Anomalous Regions With RSL Unexplained by the Model

Figure 15 displays the location of RSL sites which have data that apparently cannot be matched regardless of any adjustments in local ice cover or changes in radial earth structure. These 28 sites with data encompassing 168 separate ^{14}C age determinations can be divided into two categories, of which the first consists of sites with suspect data or which are surrounded by other sites which are well matched by the predictions of ICE-3G (denoted by the solid circles in Figure 15). The second category of sites is more difficult to explain. The characteristic which relates these sites (denoted by the triangles in Figure 15) is that of a sharply descending RSL curve, and they are exclusively found at ice marginal sites with mountainous terrain and deep and steep-sided fiords. *Clark* [1976] suggested that once the gravitational influence of the Greenland Ice Sheet, for example, was properly included in the RSL calculation then these steep curves would be correctly predicted; but this is obviously not the case. The observed and theoretically predicted responses at six of the 13 such sites that have been identified are presented in Figure 16. Obviously the LVZ model does not aid in understanding the mechanism responsible for these steep curves (dashed lines), as it, in fact, flattens the predicted RSL curves. At present, no combination of ice history adjustments and radial earth model modifications that we can imagine will explain these thirteen steep RSL curves. The data are not of particularly high quality, particularly that from Greenland which were collected over 20 years ago. Of the four Greenland RSL histories presented on Figure 16, three (Sondre Stomfjord, Skeldal, and King Frederick VIII Land) were constructed from individual samples which contained multiple shells from several different species (the lone exception is the youngest sample from Sondre Stomfjord which was a piece of driftwood). The two oldest samples from the Mesters Vig site were also multiple shells, while the four youngest samples were all pieces of driftwood. The dating of multiple shells does not allow an accurate determination of age due to possible contamination by anomalous shells and probable reworking of the shells. The use of driftwood may not allow a confident estimate of elevation or age. As mentioned previously, the sample of choice in constructing RSL curves is a whole bivalve shell found insitu.

Unfortunately, not all 13 of the sharply descending RSL curves can be written off by appealing to poor data quality. The two central Norwegian sites shown in Figure 16 are based on much more recently collected samples (i.e., in the early 1980s), and hence more confidence in the RSL history from these sites may be assumed. The Frosta data are based on the dating of the interface between lacustrine sediments and brackish sediments in proglacial lakes; the Verdalsoya data are based on molluscs occurring in marine terraces. It is interesting to note that these more recent curves are somewhat less steep than the sharply-descending RSL histories from Greenland, and they are well matched by the ICE-3G predicted RSL history for at least the last 9000 years.
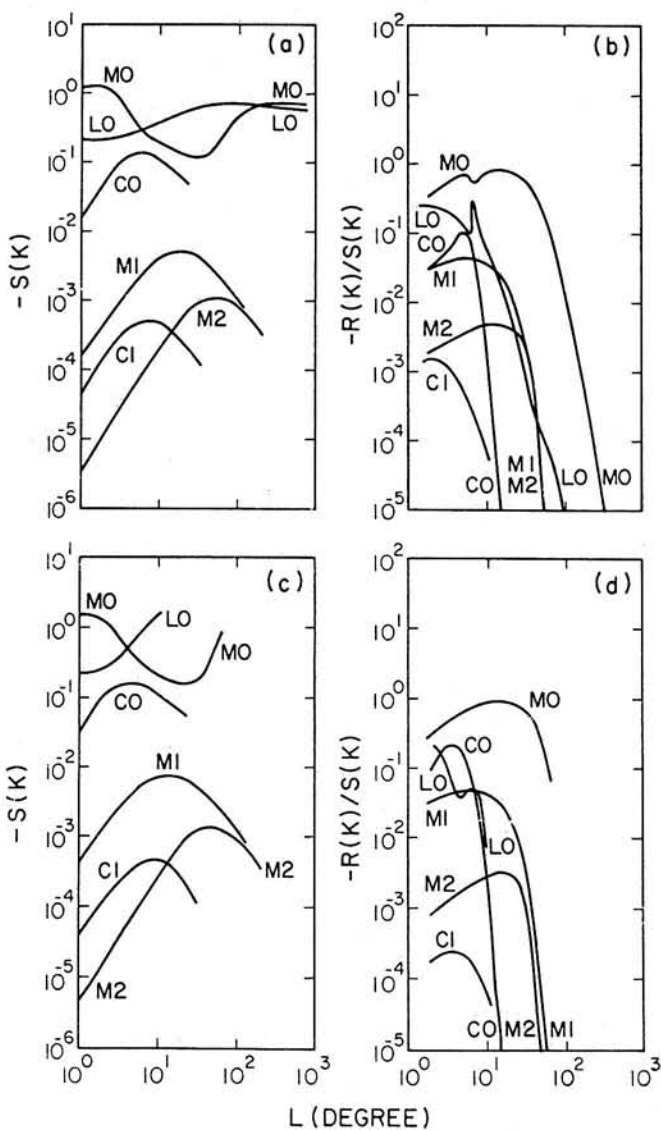

Fig. 14. Inverse relaxation time (Figures 14a and 14c) and amplitude spectra (Figures 14b and 14d) for the standard model (top) and the low viscosity zone model (bottom). Core, mantle and lithosphere fundamental modes are labelled CO, MO, and LO, respectively, and higher modes are labelled C1, M1, and M2, respectively.
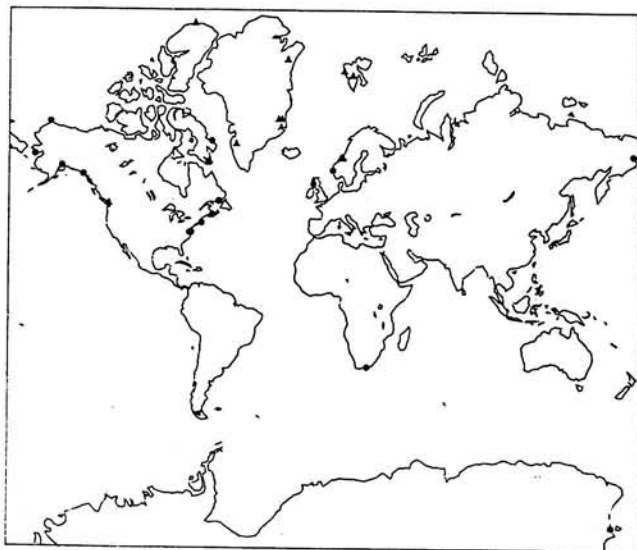

Fig. 15. Map of anomalous RSL sites. The triangles represent sites which have a sharply descending RSL curve and the dots represent sites which have suspect data or otherwise anomalous.
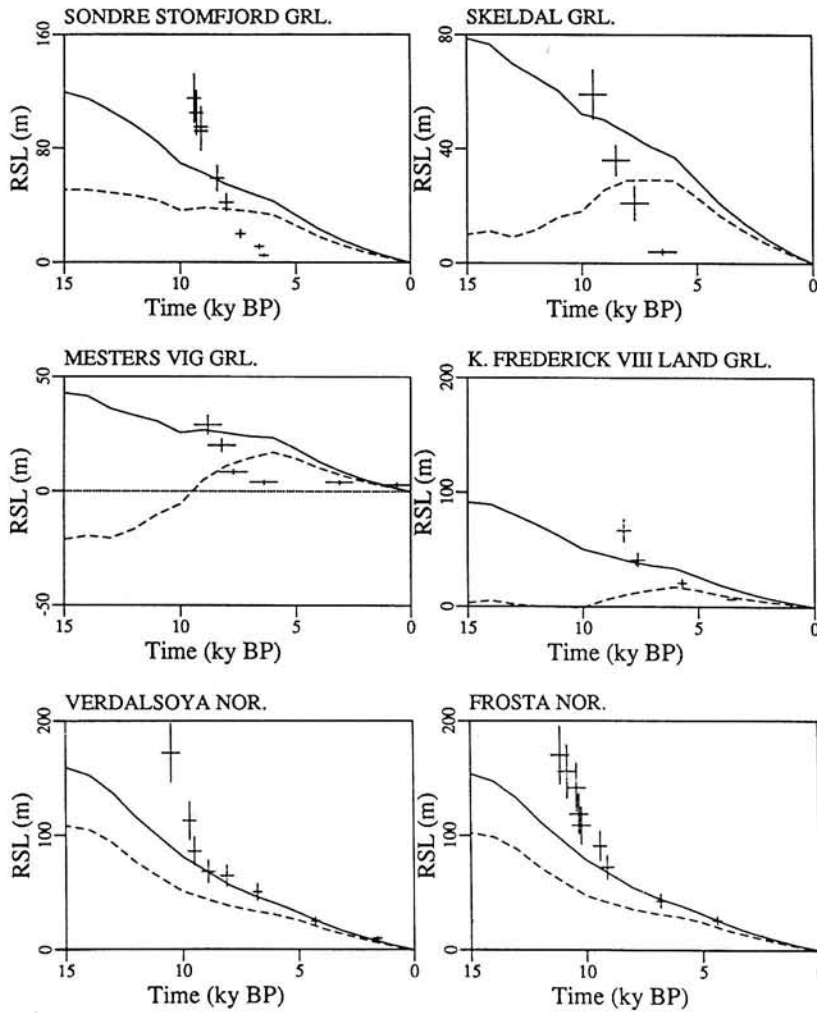
Fig. 16. RSL predictions for a sample of sites which have sharply descending RSL curves. Neither the standard or the low-viscosity zone models adequately predicted the data for these sites.
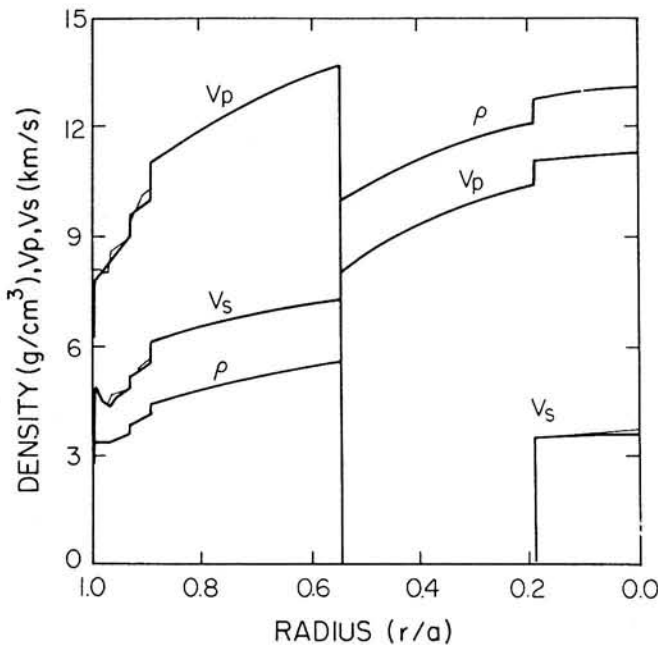

Fig. 17. Elastic structure of the Earth model. The thick lines represent the 1066B model and the thin lines represent the PREM model. V_p, V_s, and ρ are the P wave velocity, S wave velocity, and the density, respectively.

4.5. Influence of Radial Elastic Structure

In this final analysis of the sensitivity of the RSL predictions of ICE-3G the seismically determined 1066B model of the radial elastic structure employed in the standard model was compared to another seismically determined model called the Preliminary Reference Earth Model (PREM) of *Dziewonski and Anderson* [1981]. As illustrated in Figure 17, the models do not differ by much, and one would expect the RSL predictions based on these models to be quite similar. The mantle viscosity contrast and the lithospheric thickness were set at 2 and 120 km, respectively. Tables 9 and 10 compare the PREM and 1066B models by presenting the variance calculation for sites inside and outside the ice margin, respectively. As expected, due to the similarity of the models, the variances for each region are almost identical, with only a very slight preference shown for the 1066B model. The small differences in responses would be due to the different elastic structure in the upper mantle of the PREM model (sample figures are not shown since the RSL curves for PREM are either identical or very nearly so to those of 1066B).

5. SUMMARY

The work presented here has had a three fold purpose: (1) First, we compile in a single source all available relative sea level data (including previously unpublished data from Thores River,

TABLE 9. Variance Statistics for the PREM Model

Region	Number of Sites	Number of Data	Variance		
			PREM	1066B	Minimum
Arctic Canada and Greenland	69	365	0.76	0.75	1.09
Northern Europe	73	397	0.62	0.61	0.59
Eastern North America	25	152	1.34	1.32	1.71
Southern Europe	2	11	2.01	1.93	1.41
Atlantic, Indian, and Southern Oceans	5	16	3.14	3.12	1.43
Pacific Ocean	17	69	3.14	3.12	1.43
Global	191	1010	0.47	0.47	0.53

For RSL sites inside the ICE-3G Margin. Sites which are PREM preferred = 16 neutral = 102 1066B preferred = 73. PREM fits 53.4% of the sites within the minimum variance and 79.6% within twice the minimum variance. 1066B fits 54.5% of the sites within the minimum variance and 80.6% within twice the minimum variance.

TABLE 10. Variance Statistics for the PREM Model

Region	Number of Sites	Number of Data	Variance		
			PREM	1066B	Minimum
Arctic Canada and Greenland	0	0	0.00	0.00	0.00
Northern Europe	13	46	0.48	0.48	0.68
Eastern North America	34	175	0.91	0.90	0.68
Southern Europe	24	102	0.62	0.62	0.49
Atlantic, Indian, and Southern Oceans	65	254	0.34	0.34	0.35
Pacific Ocean	65	303	0.50	0.49	0.21
Global	201	880	0.28	0.28	0.20

For RSL sites outside the ICE-3G Margin. Sites which are PREM preferred = 45 neutral = 107 1066B preferred = 52. PREM fits 53.7% of the sites within the minimum variance and 81.6% within twice the minimum variance. 1066B fits 53.7% of the sites within the minimum variance and 81.6% within twice the minimum variance.

Ellesmere Island, Canada). It is hoped that this comprehensive data base of 392 globally distributed sites may provide the raw material for subsequent analyses by many scientists from a variety of research fields. (2) Using a subset of 200 sites taken from the complete data base which were not employed in the construction of the deglaciation model (as described by *Tushingham and Peltier* [1991]), the ICE-3G model was established as globally consistent since the ICE-3G global variance for this subset of the data was shown to be significantly less than the global variance for the previous lower resolution model ICE-2. (3) The sensitivity of the isostatic response to changes in the earth model was assessed.

It was observed that the response was relatively insensitive to changes in lithospheric thickness at ice central and far-field sites (as the former are sensitive to deep-earth structure and the latter are principally sensitive only to the redistribution of meltwater) but very sensitive at the ice-marginal sites. A lithospheric thickness of 245 km was found to be preferred by marginal sites, particularly

for sites along the eastern coast of the United States, although significant unexplained misfits to the data at these locations remain. The RSL histories at far-field sites were also found to be very weakly sensitive to changes in the mantle viscosity contrast across the 670-km seismic discontinuity, but this was not found to be the case elsewhere. Not surprisingly a contrast of a factor of 2 between viscosities of the upper and lower mantles was preferred by RSL sites that were used to construct the ICE-3G model, but there was no clear preference by sites located outside the ice margin for models with contrasts between 2 and 4. The model with a very high contrast of 1000, although very slightly preferred over the low contrast model at a small number of sites in the far field, could easily be discounted for physical reasons outlined in section 4.2. Further, the uniform model incorrectly predicted raised beaches along the southeastern U.S. coast which are not observed. These arguments lead to the conclusion that the upper mantle-lower mantle viscosity contrast is somewhere between a

factor of 2 and a factor of 4 when the upper mantle viscosity is fixed to the 10^{21} Pa s value required by the data from Fennoscandia. A model with a low viscosity zone beneath the lithosphere was also tested and was found not to be favoured anywhere except marginally along the European coast from West Germany to Britanny. The sensitivity to realistic changes in the density and elastic structure of the Earth, allowed by seismological data, was found to be negligible.

In pursuing these analyses we have discovered two characteristic classes of misfits of the data to the predictions of ICE-3G, namely, those revealed by paleoshorelines of age greater than 5 kyr from along the east coast of the United States and those revealed by paleoshorelines of age greater than 9 kyr from the coasts of Greenland and Norway in deeply fiorded terrain. These are the only evidence that we have discovered in the global data base for the possible importance of lateral variations of viscosity. Whether such variations will be required to explain these "anomalous" data or whether other influences are at work will clearly require further investigation to discover.

REFERENCES

Bard, E., B. Hamelin, R.G. Fairbanks, and A. Zindler, Calibration of ^{14}C over the last 30,000 years using U/Th Ages obtained by Mass Spectrometry on Barbados Coral, *Nature*, *345*, 405-410, 1990.

Beukens, R.P., Radiocarbon analysis, 1984 annual report, pp. 31-64, 1984, Isotrace, University of Toronto, Department of Physics, 1984.

Bird, J.B., *The Physiography of Arctic Canada*, 336 pp., The John Hopkins Press, Baltimore, Md., 1967.

Bloom, A.L., *Atlas of Sea-Level Curves*, IGCP Proj. *61*, 114 pp., International Geosphere-Biosphere Programme, Royal Swedish Academy of Sciences, Stockholm, Sweden, 1977.

Clark, J.A., Greenland's rapid postglacial emergence: A result of ice-water gravitational attraction, *Geology*, *4*, 310-312, 1976.

Curray, J.R., Sediments and history of Holocene transgression, continental shelf, northwest Gulf of Mexico, in *Recent Sediments, Northwest Gulf of Mexico*, pp. 221-266, Amer. Assoc. Petrol. Geol., *221*, 1960.

Denton, G.H., and T. Hughes, *The Last Great Ice Sheet*, 484 pp., Wiley-Interscience, New York, 1981.

Dziewonski, A.M., and D.L. Anderson, Preliminary reference Earth model, *Phys. Earth Planet. Inter.*, *25*, 279-356, 1981.

England, J., Post-glacial isobases and uplift curves from the Canadian and Greeland high arctic, *Artic Alpine Res.*, *8*, 61-78, 1976a.

England, J., Late Quaternary glaciation of the eastern Queen Elizabeth Island, N.W.T., Canada: Alternative models, *Quat. Res.*, *6*, 185-202, 1976b.

England, J., Isostatic adjustments in a full glacial sea, *Can. J. Earth Sci.*, *20*, 895-917, 1983.

Fairbanks, R.G., A 17,000-year glacio-eustatic sea level record: influence of glacial melting rates on the Younger Dryas event and deep-ocean circulation, *Nature*, *342*, 637-642, 1989.

Flint, R.F., *Glacial and Quaternary Geology*, 892 pp., John Wiley, New York, 1971.

Forte, A.M., and W.R. Peltier, Plate tectonics and aspherical Earth structure: The importance of poloidal-toroidal coupling, *J. Geophys. Res.*, *92*, 3645-3679, 1987.

Forte, A.M., and W.R. Peltier, Mantle Convection and core-mantle boundary topography: Explanations and implications, *Tectonophysics*, *187*, 91-116, 1991a.

Forte, A.M., and W.R. Peltier, Viscous flow models of global geophysical observables, 1, Forward problems, *J. Geophys. Res.*, in press, 1991b.

Hager, B.H., Subducted slabs and the geoid: Constraints on mantle rheology and flow, *J. Geophys. Res.*, *89*, 6003-6015, 1984.

Gilbert, F., and A.M. Dziewonski, An application of normal mode theory to retrieval of structural parameters and source mechanisms from seismic spectra, *Philos. Trans. R. Soc. London, Ser. A*, *278*, 187-269, 1975.

Gornitz, V., S. Lebedeff, and J. Hansen, Global sea level trend in the past century, *Science*, *215*, 1611-1614, 1982.

Lemmen, D.S., The last glaciation of Marvin Peninsula, northern Ellesmere Island, High Arctic, Canada, *Can. J. Earth Sci.*, *26*, 2578-2590, 1989.

Libby, W.F., *Radiocarbon Dating*, 175 pp., Ill., University of Chicago Press, Chicago, 1955.

Litherland, A.E., H.E. Gove, and K.H. Purser, Dating with accelerators, *Phys. Today*, *33*(1), 13-15, 1980.

Olsson, I.U., and W. Blake, Jr., Problems of radiocarbon dating of raised beaches based on experience in Spitsbergen, *Nor. Geogr. Tidsskr.*, *18*, 47-64, 1962.

Pearson, G.W., J.R. Pilcher, M.G.I. Baillie, D.M. Corbett, and F. Qua, High-precision ^{14}C measurements of Irish oaks to show the natural ^{14}C variations from AD 1840 to 5210 BC, *Radiocarbon*, *28*(2B), 911-934, 1986.

Peltier, W.R., Glacial isostatic adjustment, II, The inverse problem, *Geophys. J.R. Astron. Soc.*, *46*, 669-706, 1976.

Peltier, W.R., Deglaciation-induced vertical motion of the North American Continent and transient lower mantle rheology, *J. Geophys. Res.*, *91*, 9099-9123, 1986.

Peltier, W.R., Lithospheric thickness, Antarctic deglaciation history, and ocean basin discretization effects in a global model of postglacial sea level change: A summary of some sources of non-uniqueness, *Quat. Res.*, *29*, 93-112, 1988.

Peltier, W.R., Mantle viscosity, in *Mantle Convection: Plate Tectonics and Global Dynamics* edited by W.R. Peltier, pp. 389-478, Gordon and Breach, New York, 1989.

Peltier, W.R., and J.T. Andrews, Glacial isostatic adjustment, I, The forward problem, *Geophys. J.R. Astron. Soc.*, *46*, 605-646, 1976.

Peltier, W.R., R.A. Drummond, and A.M. Tushingham, Post-glacial rebound and transient lower mantle rheology, *Geophys. J.R. Astron. Soc.*, *87*, 79-116, 1986.

Pirazzoli, P.A., J. Thommeret, Y. Thommeret, J. Laborel, and L.F. Montaggioni, Crustal block movements from Holocene shorelines: Crete and Antikythira (Greece), *Tectonophysics*, *86*, 27-43, 1982.

Redfield, A.C., and M. Rubin, The age of salt marsh peat and its relation to recent changes in the sea level at Barnstable, Massachusetts, *Proc. Natl. Acad. Sci. U.S.A.*, *48*, 1728-1735, 1962.

Richards, M.A., and B.H. Hager, Geoid anomalies in a dynamics earth, *J. Geophys. Res.*, *89*, 5987-6002, 1984.

Schackleton, N.J., A. Berger, and W.R. Peltier, An alternative astronomical calibration of the lower Pleistocene timescale based upon ODP site 677, *Trans. R. Soc. Edinburgh*, *81*, 251-261, 1990.

Stuiver, M., G.W. Pearson, and T.F. Braziunas, Radiocarbon age calibration of marine samples back to 9000 cal. yr. bp., *Radiocarbon*, *28*(2B), 980-1021, 1986.

Taira, K., Holocene crustal movements in Taiwan as indicated by radiocarbon dating of marine fossils and diftwood, *Tectonophysics*, *28*, T1-T5, 1975.

Tushingham, A.M., and W.R. Peltier, ICE-3G: A new model of late Pleistocene deglaciation based upon geophysical predictions of post-glacial sea level change, *J. Geophys. Res.*, *96*, 4497-4523, 1991.

Walcott, R.I., Late Quaternary vertical movements in eastern North America: Quantitative evidence of glacial-isostatic rebound, *Rev. Geophys.*, *10*, 849-884, 1972.

Washburn, A.L., and M. Stuiver, Radiocarbon-dated post-glacial deleveling in northeast Greenland and its implications, *Arctic*, *15*, 66-73, 1962.

Wu, P., and W.R. Peltier, Glacial isostatic adjustment and the free air gravity anomaly as a constraint on deep mantle viscosity, *Geophys. J.R. Astron. Soc.*, *74*, 377-450, 1983.

W.R. Peltier, Department of Physics, University of Toronto, Toronto, Ontario, Canada M5S 1A7.

A.M. Tushingham, Geodynamics Section, Geological Survey of Canada, 1 Observatory Crescent, Ottawa, Ontario, Canada K1A OY3.